Editors' Suggestion | Featured in Physics

QCD Constraints on Isospin-Dense Matter and the Nuclear Equation of State

Ryan Abbott,[1,2] William Detmold,[1,2] Marc Illa,[3] Assumpta Parreño,[4] Robert J. Perry,[4] Fernando Romero-López,[1,2] Phiala E. Shanahan,[1,2] and Michael L. Wagman[5]

(NPLQCD Collaboration)

[1]*Center for Theoretical Physics, Massachusetts Institute of Technology, Cambridge, Massachusetts 02139, USA*
[2]*The NSF AI Institute for Artificial Intelligence and Fundamental Interactions*
[3]*InQubator for Quantum Simulation (IQuS), Department of Physics, University of Washington, Seattle, Washington 98195, USA*
[4]*Departament de Física Quàntica i Astrofísica and Institut de Ciències del Cosmos, Universitat de Barcelona, Martí i Franquès 1, E08028, Spain*
[5]*Fermi National Accelerator Laboratory, Batavia, Illinois 60510, USA*

(Received 19 July 2024; revised 30 September 2024; accepted 22 October 2024; published 6 January 2025)

Understanding the behavior of dense hadronic matter is a central goal in nuclear physics as it governs the nature and dynamics of astrophysical objects such as supernovae and neutron stars. Because of the nonperturbative nature of quantum chromodynamics (QCD), little is known rigorously about hadronic matter in these extreme conditions. Here, lattice QCD calculations are used to compute thermodynamic quantities and the equation of state of QCD over a wide range of isospin chemical potentials with controlled systematic uncertainties. Agreement is seen with chiral perturbation theory when the chemical potential is small. Comparison to perturbative QCD at large chemical potential allows for an estimate of the gap in the superconducting phase, and this quantity is seen to agree with perturbative determinations. Since the partition function for an isospin chemical potential μ_I bounds the partition function for a baryon chemical potential $\mu_B = 3\mu_I/2$, these calculations also provide rigorous nonperturbative QCD bounds on the symmetric nuclear matter equation of state over a wide range of baryon densities for the first time.

DOI: 10.1103/PhysRevLett.134.011903

The determination of the internal structure of neutron stars presents a long-standing and important challenge for nuclear theory. Since neutron stars were first predicted in the 1930s and observed 30 years later, many models for the structure of their interiors have been proposed, including various phases of nuclear matter, mesonic condensates and hyperonic matter, and deconfined quark cores [1–6]. As observational data and terrestrial probes of the relevant nuclear densities are not sufficiently constraining, most of these possibilities for the neutron star equation of state (EOS) remain viable. From a theoretical perspective, it is expected that neutron star interiors can be described by the standard model of particle physics, however, in a regime where the strong interactions are nonperturbative. The numerical technique of lattice quantum chromodynamics (LQCD) is applicable at such large couplings, but is beset by a notorious sign problem at nonzero baryon chemical potential [7] prohibiting its direct application. Consequently, theoretical approaches to the nuclear EOS are based on models and interpolations between phenomenological constraints from nuclear structure and perturbative QCD (pQCD) calculations that are valid at asymptotically large chemical potentials (see, for example, Refs. [8–18]). In light of this, any rigorous information that can impact such analyses is of paramount importance.

In this Letter, the first nonperturbative QCD constraint on the nuclear EOS with complete quantification of systematic uncertainties is presented. These calculations build upon the proof-of-principle, single lattice spacing results of Ref. [19] with improved methodology, increased statistical precision, an extrapolation to the continuum limit, and an interpolation to the physical quark masses, enabling a systematically controlled result to be achieved for the first time. The pressure and other thermodynamic properties of low-temperature isospin-dense matter are determined over a wide range of densities and chemical potentials, spanning all scales from hadronic to perturbatively coupled. At small values of the isospin chemical potential μ_I, the results agree with chiral perturbation theory (χPT) [20,21] at next-to-leading order (NLO) [22,23]. At large μ_I, the results are seen to agree with pQCD with pairing

contributions [24]. The comparison of next-to-next-to-leading-order (NNLO) pQCD predictions [24–29] for the pressure (partial next-to-next-to-next-to-leading-order results are also available [30]) with the continuum limit of the LQCD calculations provides a determination of the superconducting gap as a function of μ_I. This is seen to agree with the leading-order perturbative calculation of the pairing gap [24], but is more precise. The speed of sound in isospin-dense matter is also seen to significantly exceed the conformal limit of $c_s^2/c^2 \leq 1/3$ over a wide range of μ_I. A Bayesian model-mixing approach that combines χPT, LQCD, and pQCD provides a determination of the zero-temperature EOS for isospin-dense QCD matter valid at all values of the isospin chemical potential.

These results provide constraints for phenomenological frameworks seeking to describe the QCD phase diagram [31], and from simple path-integral relations [32–35], the determination of the pressure in isospin-dense matter provides a nonperturbative, model-independent bound on the pressure of isospin-symmetric QCD matter at nonzero baryon chemical potential and hence on the nuclear EOS. The current results therefore provide a systematically controlled QCD bound at all densities, and the impact on nuclear phenomenology is briefly discussed.

Thermodynamic relations—Thermodynamic quantities are accessed in this Letter by building an approximation to the grand canonical partition function valid at low temperature. The grand canonical partition function is defined at a temperature $T = 1/\beta$ and isospin chemical potential μ_I by

$$Z(\beta, \mu_I) = \sum_s e^{-\beta(E_s - \mu_I I_z(s))}, \tag{1}$$

where the sum is over all states s, and E_s and $I_z(s)$ correspond to the energy and z component of the isospin of a given state, respectively. Since states of different I_z but the same I are approximately degenerate, contributions from states with $I_z < I$ are suppressed by $\mathcal{O}(e^{-\beta\mu_I})$ relative to those with $I_z = I$ and can therefore be neglected. Additionally, only the ground state for each isospin contributes at low temperature. The summation can therefore be approximated in terms of these $I_z = I$ ground states, which can be labeled by their isospin charge $n = I = I_z$, and truncated at some $n_{\max}$ giving

$$Z(\beta \to \infty, \mu_I) \simeq \sum_{n=0}^{n_{\max}} e^{-\beta(E_n - \mu_I n)}. \tag{2}$$

$E_0 = 0$ is chosen, and this approximation is valid for values of μ_I such that the truncation at $n_{\max}$ does not affect the result significantly.

For an observable $\mathcal{O}$ that only depends on the energy and isospin charge of the system, the thermodynamic expectation value of $\mathcal{O}$ can be computed as

$$\langle \mathcal{O}(E,n) \rangle_{\beta,\mu_I} = \frac{1}{Z(\beta,\mu_I)} \sum_n \mathcal{O}(E_n, n) e^{-\beta(E_n - \mu_I n)}. \tag{3}$$

The energy density can be computed using the quantity E_n/V, while the isospin-charge density can be computed from the expectation value of n/V, where V is the volume of the system. Derivatives of observables can also be computed using

$$\frac{\partial}{\partial \mu_I} \langle \mathcal{O} \rangle_{\beta,\mu_I} = \beta \left(\langle n\mathcal{O} \rangle_{\beta,\mu_I} - \langle n \rangle_{\beta,\mu_I} \langle \mathcal{O} \rangle_{\beta,\mu_I} \right), \tag{4}$$

which results from directly differentiating Eq. (3). This leads to the following expressions for the pressure,

$$P(\beta, \mu_I) = \int_0^{\mu_I} \frac{\langle n \rangle_{\beta,\mu}}{V} d\mu, \tag{5}$$

and speed of sound defined by the isentropic derivative of the pressure with respect to the energy density ϵ,

$$\frac{1}{c_s^2} = \frac{\partial \epsilon}{\partial P} = \frac{1}{\langle n \rangle_{\beta,\mu_I}} \frac{\partial}{\partial \mu_I} \langle E \rangle_{\beta,\mu_I}. \tag{6}$$

Previous work [19,36–39] studied isospin-dense matter through a canonical partition function approach by using the thermodynamic relation

$$\mu_I = \frac{dE_n}{dn} \tag{7}$$

to determine the isospin chemical potential from the extracted energies. Other studies have added the isospin chemical potential directly to the QCD action [40–44]. These studies probe isospin-dense QCD at $\mu_I \lesssim 2$ and focus primarily on nonzero temperature. The results in this Letter are consistent with the low-temperature results in those works, but span a larger range of chemical potentials.

The primary advantage of the method used here in comparison to the method of Ref. [19] is that μ_I enters as an input to the calculation of thermodynamic quantities rather than being derived from the isospin charge of the LQCD data and therefore is not subject to statistical and systematic uncertainties. A more detailed comparison to the approach of Ref. [19] is discussed in the Supplemental Material [45].

Color-superconducting gap—At large isospin chemical potential, asymptotic freedom guarantees the validity of pQCD and the resulting prediction of a color-singlet superconducting state at zero temperature [20]. In this state, Cooper pairs of quark–anti-quark fields condense, leading to a superconducting gap with order parameter $\langle \bar{d}_a \gamma_5 u_b \rangle = \delta_{ab}\Delta$, where a and b are color indices. The gap Δ can be computed perturbatively [20,24], with the next-to-leading order result given by

$$\Delta = \tilde{b}\mu_I \exp\left(-\frac{\pi^2 + 4}{16}\right) \exp\left(-\frac{3\pi^2}{2g}\right), \tag{8}$$

where $\tilde{b} = 512\pi^4 g^{-5}$, and $g = \sqrt{4\pi\alpha_s(\mu_I)}$ is the strong coupling at the scale μ_I. Notably, the prefactor of $1/g$ in the

exponent of Eq. (8) is smaller than the analogous coefficient in the baryon-density case by a factor of $1/\sqrt{2}$ [20], leading to an exponential enhancement of the gap and its effects in isospin-dense QCD. If pQCD is reliable for a given μ_I and $\mu_B = 3\mu_I/2$, then the isospin-dense gap bounds the baryonic gap, in which there is significant phenomenological interest [46].

The nontrivial background in the presence of the gap induces a change in the pressure of the system. This change can be computed perturbatively, as has been done at NLO in Ref. [24] with the result

$$\delta P \equiv P(\Delta) - P(\Delta = 0) = \frac{N_c}{2\pi^2}\mu_I^2\Delta^2\left(1 + \frac{g}{6}\right). \quad (9)$$

This difference allows for an indirect extraction of the gap by comparing the lattice QCD pressure with the pressure derived in pQCD without pairing.

LQCD calculations—Following the methods and analysis techniques developed in Ref. [19], the energies of systems of isospin charge $n \in \{1, \ldots, 6144\}$ are determined from two-point correlation functions

$$C_n(t) = \left\langle \left(\sum_{\mathbf{x}} \pi^-(\mathbf{x}, 0)\right)^n \prod_{i=1}^{n} \pi^+(\mathbf{y}_i, t) \right\rangle \quad (10)$$

calculated on four ensembles of gauge-field configurations whose parameters are shown in Table I. Here, $\pi^-(\mathbf{x}, t) = \pi^+(\mathbf{x}, t)^\dagger = -\bar{d}(\mathbf{x}, t)\gamma_5 u(\mathbf{x}, t)$ is an interpolating operator built from u and d quark fields that creates states with the quantum numbers of the π^-. The correlation functions are computed using the symmetric polynomial method of Ref. [19] from sparsened [47] quark propagators computed using a grid of 512 source locations on a single time slice of each configuration.

The relevant ground-state energies E_n are determined from an analysis of the t dependence of the effective energy functions

$$aE_n^{\text{eff}}(t) = \log\frac{C_n(t)}{C_n(t-1)} = \vartheta_n(t) - \vartheta_n(t-1) + \frac{\sigma_n^2(t)}{2} - \frac{\sigma_n^2(t-1)}{2}, \quad (11)$$

where a is the lattice spacing, $\vartheta_n(t)$ and $\sigma_n(t)$ are the mean and standard deviation of $\log C_n(t)$, and the second equality is under the assumption of log-normality [19]. $N_b = 2000$ bootstrap resamplings are used on each ensemble to assess the statistical uncertainties and address correlations. As in Ref. [19], on each bootstrap the energy is given by the value of the effective mass on a randomly chosen time inside the effective mass plateau region.

Given the energies determined on each ensemble for systems of isospin charge $n \in \{1, \ldots, 6144\}$, Eqs. (5) and (6) are used to determine the pressure, the energy density, and speed of sound. The action used in these calculations is perturbatively improved, so discretization effects are $\mathcal{O}(a^2, g^2 a)$. The mass dependence of quantities evaluated over the range of quark masses used in the calculations is expected to be described linearly in $m_{ud} \sim m_\pi^2$. Each quantity $X \in \{P/P_{\text{SB}}, \epsilon/\epsilon_{\text{SB}}, c_s^2/c^2\}$ (where $P_{\text{SB}} = \epsilon_{\text{SB}}/3 = \mu_I^4/32\pi^2$ is the pressure of a Stefan-Boltzmann gas) is fit with forms including arbitrary μ_I dependence and terms $\mathcal{O}(a^2, a^2\mu_I, a^2\mu_I^2, (m_\pi^2 - \bar{m}_\pi^2))$, where $\bar{m}_\pi = m_{\pi^+} = 139.57039$ MeV [52], with coefficients independent of μ_I. The systematic uncertainty from the extrapolation is assessed by combining fits with all possible subsets of the terms above through model averaging [53–55]. The systematic uncertainty and the statistical uncertainty are combined under the bootstrap procedure. The lattice determinations of the pressure, energy density, and speed of sound are shown in the Supplemental Material [45], along with further details.

The calculated pressure is shown in Fig. 1 for each lattice ensemble as well as for the continuum-limit, physical-quark-mass interpolation. The LQCD results for the different volumes, lattice spacings, and quark masses used in the calculations are seen to agree with each other within uncertainties and also with the physical mass, continuum-limit extraction. The LQCD pressure agrees with NLO χPT at small values of the chemical potential and can be compared with NNLO pQCD [24–29] at large values of the chemical potential. The mild tension seen between LQCD and pQCD for $\mu_I \in [1500, 2250]$ MeV potentially indicates the presence of a superconducting gap [24]

TABLE I. Parameters of the gauge-field configurations used in this Letter. Ensembles were generated with $N_f = 2 + 1$ flavors of quarks using a clover fermion action [48] and a tree-level improved Lüscher-Weisz gauge action [49]. The first column lists the label used to refer to the ensemble, N_{conf} is the number of configurations, and β_g and C_{SW} refer to the gauge coupling and clover coefficient, respectively. The lattice spacing a is determined in Refs. [50,51], while the lattice geometries are defined by the spatial and temporal extents L and L_4, respectively. The bare light (up and down, m_{ud}) and strange (m_s) quark masses are given in lattice units, and m_π is the pion mass. The temperature $T = 1/(aL_4)$ is also shown.

Label	N_{conf}	β_g	C_{SW}	am_{ud}	am_s	$(L/a)^3 \times (L_4/a)$	a (fm)	m_π (MeV)	L (fm)	$m_\pi L$	T (MeV)
A	665	6.3	1.205 37	−0.2416	−0.2050	$48^3 \times 96$	0.091(1)	169(3)	4.37	3.75	22.8
B	1262	6.3	1.205 37	−0.2416	−0.2050	$64^3 \times 128$	0.091(1)	169(2)	5.82	5.08	17.1
C	846	6.5	1.170 08	−0.2091	−0.1778	$72^3 \times 192$	0.070(1)	164(3)	5.04	4.33	14.7
D	977	6.5	1.170 08	−0.2095	−0.1793	$96^3 \times 192$	0.070(1)	125(4)	6.72	4.40	14.7

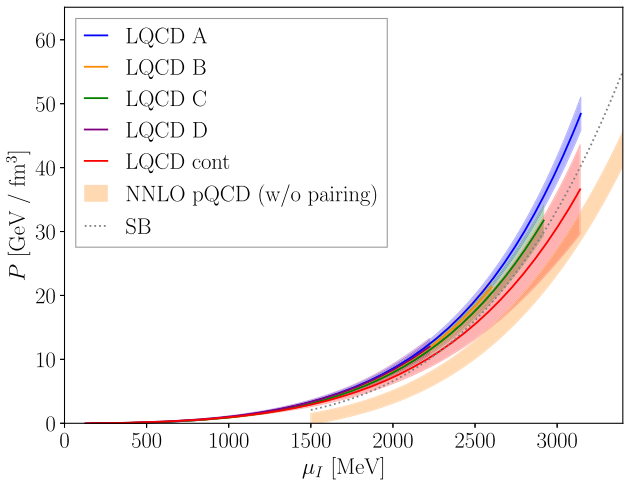

FIG. 1. The pressure computed for each LQCD ensemble as well as for the continuum-limit, physical mass extraction. Results from the Stefan-Boltzmann limit of a free Fermi gas and from NNLO pQCD without pairing or quark mass effects are shown for $\mu_I \gtrsim 1500$ MeV.

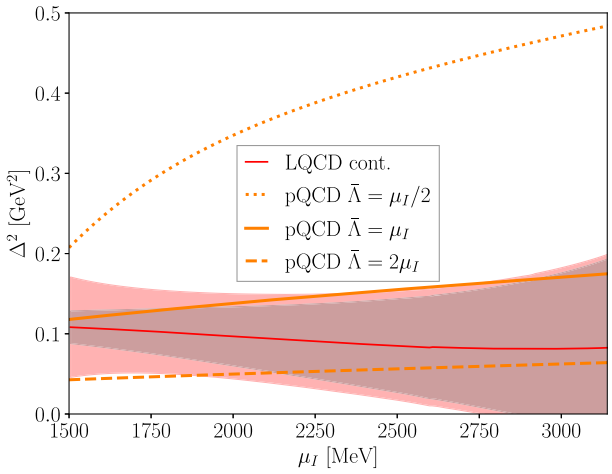

FIG. 2. Comparison of the pQCD form in Eq. (8) for the BCS gap (orange curves evaluated at scales $\bar{\Lambda} = \mu_I \times \{0.5, 1.0, 2.0\}$) with that determined from the difference between the continuum limit of LQCD calculations and the NNLO pQCD result (red curve). The inner shaded error region is the extrapolated LQCD uncertainty, while the outer shaded error region combines this with the NNLO pQCD uncertainty.

(it could alternatively be an indication of the breakdown of pQCD, although NLO and NNLO pQCD results are in agreement over this range).

The corresponding speed of sound is seen to exceed the conformal limit of $c_s^2/c^2 = 1/3$ over a wide range of the isospin chemical potential (see Fig. 3 below). While this behavior was seen in Refs. [19,44,56] (and also in two-color QCD [57,58]), the present results confirm that this is not a lattice artifact and that such a behavior is possible in strongly interacting QCD matter. This suggests that the assumption that the speed of sound remains below this value in baryonic matter is questionable.

Given the LQCD calculation of the pressure, a determination of the superconducting gap can be made by subtracting the pQCD calculation of the pressure in the absence of the gap. In the range of chemical potentials where pQCD is a controlled expansion, this determines the gap, accurate to the same order as the perturbative subtraction. Figure 2 shows the extracted gap found using the NNLO pQCD pressure subtraction as well as a comparison to the pQCD gap in Eq. (8) evaluated at scales $\bar{\Lambda} = \mu_I \times \{0.5, 1.0, 2.0\}$ as a guide to uncertainty. As can be seen, the gap extracted from the LQCD calculations is in agreement with the perturbative gap for $\mu_I \in [1500, 3250]$ MeV but is considerably more precisely determined than the uncertainty from perturbative scale variation. Since there is agreement with the perturbative estimate, the gap is also most likely larger than the corresponding gap for baryonic matter.

Equation of state for isospin-dense mater—The continuum-limit lattice QCD calculations presented above span isospin chemical potentials from just above the pion mass to values where pQCD appears to converge. Consequently, by combining the LQCD results with χPT and pQCD, the zero-temperature EOS of isospin-dense matter can be described for all μ_I with uncertainties quantified using Bayesian inference. The functional dependence of each overlapping theoretical constraint on μ_I is modeled by a correlated Gaussian distribution. The ensemble of constraints is combined via a Gaussian process (GP), following similar work for the nuclear EOS [9,59–61]. Theoretical uncertainties of χPT are estimated from the difference between the NLO and LO results, and uncertainties in pQCD are assessed from scale variation over $\bar{\Lambda} \in \mu_I \times [0.5, 2.0]$. Figure 3 shows the GP-model results for the

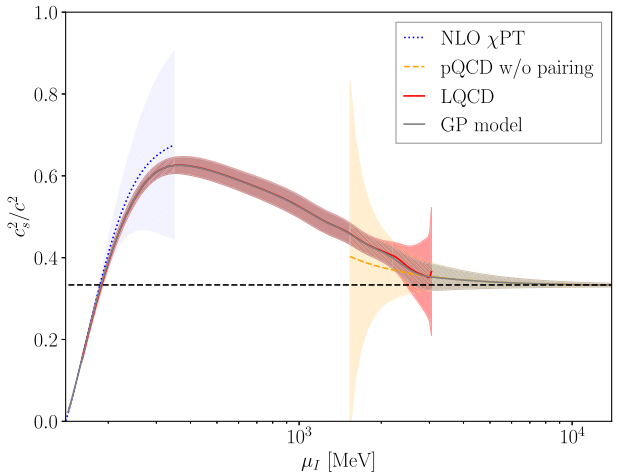

FIG. 3. The squared speed of sound as a function of the isospin chemical potential. The lattice QCD determination (red), pQCD determination (orange), and χPT determination (blue) are combined into the GP model (gray) as discussed in the main text. The dashed horizontal line shows the conformal limit.

speed of sound in comparison to the three theoretical inputs. A data file for evaluating this model accompanies this article. With a complete quantification of the isospin-dense equation of state, phenomenological implications such as the existence of pion stars [62–64] and the isospin effects that distinguishes pure neutron matter from symmetric nuclear matter [65,66] can be further investigated.

Constraining the nuclear equation of state—The partition function of two-flavor QCD with an isospin chemical potential μ_I can be written in terms of the path integral

$$Z_I(\beta,\mu_I) = \int_\beta [dA] \det \mathcal{D}\left(-\frac{\mu_I}{2}\right) \det \mathcal{D}\left(\frac{\mu_I}{2}\right) e^{-S_G} = \int_\beta [dA] \left|\det \mathcal{D}\left(\frac{\mu_I}{2}\right)\right|^2 e^{-S_G}, \quad (12)$$

where A is the gluon field, $\mathcal{D}(\mu) \equiv \not{D} + m - \mu_q \gamma_0$ is the Dirac operator with quark chemical potential μ_q, S_G is the gauge action, and $\int_\beta [dA]$ indicates integration over gauge fields with period β in the temporal direction. As first shown in Refs. [32,33], this partition function bounds the partition function of two-flavor QCD with equal chemical potentials for u and d quarks

$$Z_B(\beta,\mu_B) = \int_\beta [dA] \mathrm{Re}\left[\det \mathcal{D}\left(\frac{\mu_B}{N_c}\right)\right]^2 e^{-S_G} \quad (13)$$

as

$$Z_B(\beta,\mu_B) \leq Z_I\left(\beta, \mu_I = \frac{2\mu_B}{N_c}\right). \quad (14)$$

By the monotonicity of the logarithm, the above inequality directly translates into an inequality between the pressures of the two media as a function of the energy density. Consequently, the isospin-dense EOS bounds the EOS for symmetric nuclear matter. At large values of the quark chemical potentials, where pQCD is valid, this bound becomes tight as differences between the partition functions enter only at $\mathcal{O}(\alpha_s^k)$ for $k \geq 3$ [35]. This bound was explored in Ref. [34] based on the previous lattice QCD results [19] at a single lattice spacing and unphysical quark masses. Here, Fig. 4 presents updated bounds based on the continuum-limit lattice QCD results at the physical quark masses, χPT, and perturbative QCD through the GP model. While the bounds from isospin-dense matter do not significantly constrain phenomenological nuclear equations of state within the uncertainties that are typically presented [8–18], the bounds are independent of modeling uncertainties that enter the nuclear EOS in the regions that are unconstrained by nuclear structure or pQCD calculations. GP models without lattice QCD constraints result in significantly larger uncertainties in the position of the bound, in particular, in the lower right corner of the red band of Fig. 4.

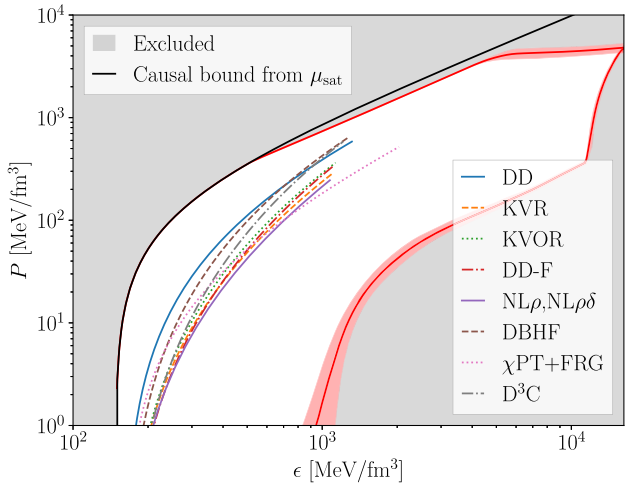

FIG. 4. The bounds on the EOS of symmetric nuclear matter derived from the GP model of the isospin-dense EOS (an EOS that enters this region would not be consistent with QCD). The boundary of the excluded region is shown as the red band, with uncertainties propagated from the GP model. Also shown are the bound from causality and a range of phenomenological EOSs for symmetric nuclear matter: DBHF [14], DD, D^{3}C, and DD-F [15], KVOR and KVR [16], NLρ,NL$\rho\delta$ [17] (all taken from Ref. [18] for $\rho_0 < \rho < 6\rho_0$), and a χEFT + FRG interpolation [18] for $\rho_0 < \rho < 10\rho_0$.

Summary—In this Letter, a determination of the equation of state of isospin-dense matter for the complete range of isospin chemical potential at zero temperature is presented for the first time. To achieve this, continuum-limit LQCD calculations are combined with pQCD calculations and χPT through a model-mixing approach in overlapping regions of isospin chemical potential. Comparison to pQCD enables a determination of the superconducting gap, and QCD inequalities translate the isospin-dense EOS into rigorous bounds on the nuclear EOS relevant for astrophysical environments.

Acknowledgments—We are grateful to Yuki Fujimoto and Sanjay Reddy for discussions. The ensembles used in this work were generated through the combined efforts of the JLab, William and Mary, Los Alamos, and MIT groups. We particularly thank Balint Joó for assistance with the generation of the gauge configurations and quark propagators used in this work. The calculations were performed using an allocation from the Innovative and Novel Computational Impact on Theory and Experiment program using the resources of the Oak Ridge Leadership Computing Facility located in the Oak Ridge National Laboratory, which is supported by the Office of Science of the Department of Energy under Contract No. DE-AC05-00OR22725. This research also used resources of the National Energy Research Scientific Computing Center, a U.S. Department of Energy Office of Science User Facility located at Lawrence Berkeley National Laboratory, operated

under Contract No. DE-AC02-05CH11231. We acknowledge USQCD computing allocations and PRACE for awarding us access to Marconi100 at CINECA, Italy. This work is supported by the National Science Foundation under Cooperative Agreement No. PHY-2019786 (The NSF AI Institute for Artificial Intelligence and Fundamental Interactions [67]) and by the U.S. Department of Energy, Office of Science, Office of Nuclear Physics under Grant Contract No. DE-SC0011090. R. A., W. D., and P. E. S. are also supported by the U.S. Department of Energy SciDAC5 Award No. DE-SC0023116. R. A. was also partially supported by the High Energy Physics Computing Traineeship for Lattice Gauge Theory (DE-SC0024053). F. R. L. acknowledges financial support from the Mauricio and Carlota Botton Fellowship. M. I. is partially supported by the Quantum Science Center, a National Quantum Information Science Research Center of the U.S. Department of Energy. P. E. S. is also supported by the U.S. DOE Early Career Award No. DE-SC0021006. A. P. and R. P. acknowledge support from Grant No. CEX2019-000918-M and the Project No. PID2020–118758 GB-I00, financed by the Spanish MCIN/AEI/10.13039/501100011033/, and from the EU STRONG-2020 project under the program H2020-INFRAIA-2018-1 Grant Agreement No. 824093. This manuscript has been authored by Fermi Research Alliance, LLC under Contract No. DE-AC02-07CH11359 with the U.S. Department of Energy, Office of Science, Office of High Energy Physics. This work made use of Chroma [68], QDPJIT [69], QUDA [70,71], JAX [72], NUMPY [73], SCIPY [74], MATPLOTLIB [75], and HDF5 [76].

[1] F. Özel and P. Freire, Annu. Rev. Astron. Astrophys. **54**, 401 (2016).
[2] M. Oertel, M. Hempel, T. Klähn, and S. Typel, Rev. Mod. Phys. **89**, 015007 (2017).
[3] G. Baym, T. Hatsuda, T. Kojo, P. D. Powell, Y. Song, and T. Takatsuka, Rep. Prog. Phys. **81**, 056902 (2018).
[4] M. Mannarelli, Particles **2**, 411 (2019).
[5] G. F. Burgio, H. J. Schulze, I. Vidana, and J. B. Wei, Prog. Part. Nucl. Phys. **120**, 103879 (2021).
[6] J. M. Lattimer, Annu. Rev. Nucl. Part. Sci. **71**, 433 (2021).
[7] P. de Forcrand, Proc. Sci., LAT2009 (**2009**) 010 [arXiv:1005.0539].
[8] E. Annala, T. Gorda, J. Hirvonen, O. Komoltsev, A. Kurkela, J. Nättilä, and A. Vuorinen, Nat. Commun. **14**, 8451 (2023).
[9] A. C. Semposki, C. Drischler, R. J. Furnstahl, J. A. Melendez, and D. R. Phillips, arXiv:2404.06323.
[10] M.-Z. Han, Y.-J. Huang, S.-P. Tang, and Y.-Z. Fan, Sci. Bull. **68**, 913 (2023).
[11] J.-L. Jiang, C. Ecker, and L. Rezzolla, Astrophys. J. **949**, 11 (2023).
[12] G. Raaijmakers *et al.*, Astrophys. J. Lett. **893**, L21 (2020).
[13] S. Huth, C. Wellenhofer, and A. Schwenk, Phys. Rev. C **103**, 025803 (2021).
[14] E. N. E. van Dalen, C. Fuchs, and A. Faessler, Phys. Rev. C **72**, 065803 (2005).
[15] S. Typel, Phys. Rev. C **71**, 064301 (2005).
[16] E. E. Kolomeitsev and D. N. Voskresensky, Nucl. Phys. **A759**, 373 (2005).
[17] B. Liu, V. Greco, V. Baran, M. Colonna, and M. Di Toro, Phys. Rev. C **65**, 045201 (2002).
[18] M. Leonhardt, M. Pospiech, B. Schallmo, J. Braun, C. Drischler, K. Hebeler, and A. Schwenk, Phys. Rev. Lett. **125**, 142502 (2020).
[19] R. Abbott, W. Detmold, F. Romero-López, Z. Davoudi, M. Illa, A. Parreño, R. J. Perry, P. E. Shanahan, and M. L. Wagman (NPLQCD Collaboration), Phys. Rev. D **108**, 114506 (2023).
[20] D. T. Son and M. A. Stephanov, Phys. Rev. Lett. **86**, 592 (2001).
[21] J. B. Kogut and D. Toublan, Phys. Rev. D **64**, 034007 (2001).
[22] P. Adhikari and J. O. Andersen, Phys. Lett. B **804**, 135352 (2020).
[23] J. O. Andersen, M. Kjøllesdal, Q. Yu, and H. Zhou, arXiv:2312.13092.
[24] Y. Fujimoto, Phys. Rev. D **109**, 054035 (2024).
[25] B. A. Freedman and L. D. McLerran, Phys. Rev. D **16**, 1130 (1977).
[26] B. A. Freedman and L. D. McLerran, Phys. Rev. D **16**, 1147 (1977).
[27] B. A. Freedman and L. D. McLerran, Phys. Rev. D **16**, 1169 (1977).
[28] V. Baluni, Phys. Rev. D **17**, 2092 (1978).
[29] A. Kurkela, P. Romatschke, and A. Vuorinen, Phys. Rev. D **81**, 105021 (2010).
[30] T. Gorda, A. Kurkela, R. Paatelainen, S. Säppi, and A. Vuorinen, Phys. Rev. Lett. **127**, 162003 (2021).
[31] R. Kumar *et al.* (MUSES Collaboration), Living Rev. Relativity **27**, 3 (2024).
[32] T. D. Cohen, Phys. Rev. Lett. **91**, 032002 (2003).
[33] T. D. Cohen, arXiv:hep-ph/0304024, 10.1142/9789812775344_0009.
[34] Y. Fujimoto and S. Reddy, Phys. Rev. D **109**, 014020 (2024).
[35] G. D. Moore and T. Gorda, J. High Energy Phys. 12 (2023) 133.
[36] W. Detmold, M. J. Savage, A. Torok, S. R. Beane, T. C. Luu, K. Orginos, and A. Parreño (NPLQCD Collaboration), Phys. Rev. D **78**, 014507 (2008).
[37] W. Detmold and M. J. Savage (NPLQCD Collaboration), Phys. Rev. D **82**, 014511 (2010).
[38] W. Detmold and B. Smigielski, Phys. Rev. D **84**, 014508 (2011).
[39] W. Detmold, K. Orginos, and Z. Shi, Phys. Rev. D **86**, 054507 (2012).
[40] J. B. Kogut and D. K. Sinclair, Phys. Rev. D **66**, 014508 (2002).
[41] J. B. Kogut and D. K. Sinclair, Phys. Rev. D **66**, 034505 (2002).
[42] B. B. Brandt, G. Endrődi, and S. Schmalzbauer, Phys. Rev. D **97**, 054514 (2018).
[43] V. G. Bornyakov, A. A. Nikolaev, R. N. Rogalyov, and A. S. Terentev, Eur. Phys. J. C **81**, 747 (2021).

[44] B. B. Brandt, F. Cuteri, and G. Endrődi, J. High Energy Phys. 07 (2023) 055.
[45] See Supplemental Material at http://link.aps.org/supplemental/10.1103/PhysRevLett.134.011903 for more computational details.
[46] A. Kurkela, K. Rajagopal, and R. Steinhorst, Phys. Rev. Lett. **132**, 262701 (2024).
[47] W. Detmold, D. J. Murphy, A. V. Pochinsky, M. J. Savage, P. E. Shanahan, and M. L. Wagman (NPLQCD Collaboration), Phys. Rev. D **104**, 034502 (2021).
[48] B. Sheikholeslami and R. Wohlert, Nucl. Phys. **B259**, 572 (1985).
[49] M. Luscher and P. Weisz, Commun. Math. Phys. **98**, 433(E) (1985); **98**, 433(E) (1985).
[50] B. Yoon *et al.*, Phys. Rev. D **95**, 074508 (2017).
[51] S. Mondal, T. Bhattacharya, R. Gupta, B. Joó, H.-W. Lin, S. Park, F. Winter, and B. Yoon, Proc. Sci., LATTICE2021 (**2021**) 513 [arXiv:2201.00067].
[52] R. L. Workman *et al.* (Particle Data Group), Prog. Theor. Exp. Phys. **2022**, 083C01 (2022).
[53] E. Rinaldi, S. Syritsyn, M. L. Wagman, M. I. Buchoff, C. Schroeder, and J. Wasem, Phys. Rev. D **99**, 074510 (2019).
[54] S. R. Beane *et al.* (NPLQCD and QCDSF Collaborations), Phys. Rev. D **103**, 054504 (2021).
[55] W. I. Jay and E. T. Neil, Phys. Rev. D **103**, 114502 (2021).
[56] B. B. Brandt, F. Cuteri, and G. Endrődi, Proc. Sci., LATTICE2022 (**2023**) 144 [arXiv:2212.01431].
[57] K. Iida and E. Itou, Prog. Theor. Exp. Phys. **2022**, 111B01 (2022).
[58] K. Iida, E. Itou, K. Murakami, and D. Suenaga, J. High Energy Phys. 10 (2024) 022.
[59] J. A. Melendez, R. J. Furnstahl, D. R. Phillips, M. T. Pratola, and S. Wesolowski, Phys. Rev. C **100**, 044001 (2019).
[60] R. Essick, I. Tews, P. Landry, S. Reddy, and D. E. Holz, Phys. Rev. C **102**, 055803 (2020).
[61] D. Mroczek, M. C. Miller, J. Noronha-Hostler, and N. Yunes, arXiv:2309.02345.
[62] B. B. Brandt, G. Endrodi, E. S. Fraga, M. Hippert, J. Schaffner-Bielich, and S. Schmalzbauer, Phys. Rev. D **98**, 094510 (2018).
[63] J. O. Andersen and M. K. Johnsrud, arXiv:2206.04291.
[64] O. S. Stashko, O. V. Savchuk, L. M. Satarov, I. N. Mishustin, M. I. Gorenstein, and V. I. Zhdanov, Phys. Rev. D **107**, 114025 (2023).
[65] A. Steiner, M. Prakash, J. Lattimer, and P. Ellis, Phys. Rep. **411**, 325 (2005).
[66] B.-A. Li, L.-W. Chen, and C. M. Ko, Phys. Rep. **464**, 113 (2008).
[67] https://iaifi.org.
[68] R. G. Edwards and B. Joó, Nucl. Phys. B, Proc. Suppl. **140**, 832 (2005).
[69] F. T. Winter, M. A. Clark, R. G. Edwards, and B. Joó, in *Proceedings of the 2014 IEEE 28th International Parallel and Distributed Processing Symposium, IPDPS '14* (IEEE Press, New York, 2014), 10.1109/IPDPS.2014.112.
[70] M. A. Clark, R. Babich, K. Barros, R. Brower, and C. Rebbi, Comput. Phys. Commun. **181**, 1517 (2010).
[71] M. A. Clark, B. Joó, A. Strelchenko, M. Cheng, A. Gambhir, and R. C. Brower, in *Proceedings of the International Conference for High Performance Computing, Networking, Storage and Analysis, SC '16* (IEEE Press, New York, 2016); arXiv:1612.07873.
[72] J. Bradbury, R. Frostig, P. Hawkins, M. J. Johnson, C. Leary, D. Maclaurin, G. Necula, A. Paszke, J. VanderPlas, S. Wanderman-Milne, and Q. Zhang, http://github.com/google/jax (2018).
[73] C. R. Harris *et al.*, Nature (London) **585**, 357 (2020).
[74] P. Virtanen *et al.* (SciPy 1.0 Contributors), Nat. Methods **17**, 261 (2020).
[75] J. D. Hunter, Comput. Sci. Eng. **9**, 90 (2007).
[76] The HDF Group, https://github.com/HDFGroup/hdf5.